$\mathbb{Z}_2$ Parton Phases in the Mixed-Dimensional $t - J_z$ Model

Fabian Grusdt[1,2] and Lode Pollet[1,2,3]

[1]*Department of Physics and Arnold Sommerfeld Center for Theoretical Physics (ASC), Ludwig-Maximilians-Universität München, Theresienstr. 37, München D-80333, Germany*

[2]*Munich Center for Quantum Science and Technology (MCQST), Schellingstr. 4, D-80799 München, Germany*

[3]*Wilczek Quantum Center, School of Physics and Astronomy, Shanghai Jiao Tong University, Shanghai 200240, China*

(Received 5 August 2020; accepted 19 November 2020; published 16 December 2020)

We study the interplay of spin and charge degrees of freedom in a doped Ising antiferromagnet, where the motion of charges is restricted to one dimension. The phase diagram of this mixed-dimensional $t - J_z$ model can be understood in terms of spinless chargons coupled to a $\mathbb{Z}_2$ lattice gauge field. The antiferromagnetic couplings give rise to interactions between $\mathbb{Z}_2$ electric field lines which, in turn, lead to a robust stripe phase at low temperatures. At higher temperatures, a confined meson-gas phase is found for low doping whereas at higher doping values, a robust deconfined chargon-gas phase is seen, which features hidden antiferromagnetic order. We confirm these phases in quantum Monte Carlo simulations. Our model can be implemented and its phases detected with existing technology in ultracold atom experiments. The critical temperature for stripe formation with a sufficiently high hole concentration is around the spin-exchange energy J_z, i.e., well within reach of current experiments.

DOI: 10.1103/PhysRevLett.125.256401

Introduction.—Ultracold atoms in optical lattices provide an excellent platform to perform analog quantum simulations: they can mimic the behavior of tunable model Hamiltonians that are difficult or impossible to solve with current numerics. Since the advent of quantum simulators, an application to the 2D Fermi-Hubbard model has been a central goal: This model is believed to describe some of the most essential but theoretically poorly understood properties of strongly correlated electrons in the context of high-temperature superconductors. In the past years, significant steps have been taken towards simulating the Hubbard model, including the observation of long-range [1] and canted [2] antiferromagnetism (AFM), bad metallic [3] and spin [4] transport, magnetic polarons [5,6], string patterns [7,8], and in 1D spin-charge separation [9,10] and incommensurate magnetism [11]. Nevertheless, the critical temperatures of the expected ordered phase (stripes [12], superconductivity [13]) are too low and have not yet been reached in ultracold fermion experiments.

In this Letter we make use of the versatility of ultracold atoms to study a closely related cousin of the 2D Hubbard model. Its two main advantages are (i) significantly enhanced critical temperatures for the formation of stripe order amenable to quantum simulation and (ii) thorough theoretical understanding and numerical control of the underlying physics. Both (i) and (ii) provide a promising starting point, in experiment and theory, for a systematic exploration of the 2D Hubbard model.

Specifically, we consider a $t - J_z$ model with mixed dimensionality [14] as elucidated in Fig. 1(a),

$$\hat{\mathcal{H}} = -t \sum_{\sigma,\langle \boldsymbol{i},\boldsymbol{j}\rangle_x} \hat{\mathcal{P}}(\hat{c}^\dagger_{\boldsymbol{i},\sigma}\hat{c}_{\boldsymbol{j},\sigma} + \text{H.c.})\hat{\mathcal{P}} + J_z \sum_{\langle \boldsymbol{i},\boldsymbol{j}\rangle} \hat{S}^z_{\boldsymbol{i}}\hat{S}^z_{\boldsymbol{j}}. \quad (1)$$

The dopants (holes) are free to move only along the x direction, with tunneling rate t, while nearest-neighbor (NN) AFM Ising interactions between the spins, of strength J_z, are present along all dimensions of the lattice. In Eq. (1) $\langle \boldsymbol{i},\boldsymbol{j}\rangle$ denotes a pair of NN sites in a two-dimensional square lattice (every bond is counted once in the sum). Similarly, $\langle \boldsymbol{i},\boldsymbol{j}\rangle_x$ denotes a nearest neighbor bond oriented along the x axis. We consider a two-component mixture of particles $\hat{c}_{\boldsymbol{j},\sigma}$ with a hard-core constraint imposed by the projector $\hat{\mathcal{P}}$ onto the subspace without double occupancies. The statistics of the particles $\hat{c}_{\boldsymbol{j},\sigma}$ plays no role: By introducing Jordan-Wigner strings along the chains in the x direction one can switch between fermions and bosons.

Symmetries and mapping to $\mathbb{Z}_2$ lattice gauge theory.—Since holes cannot tunnel along y, their number N^h_y is conserved in each chain y. In the following we restrict ourselves to equal doping n_h in every chain, $N^h_y = n_h L_x$ with the system size $L_{x(y)}$ along x (y). In addition to the global $U(1)^{\otimes L_y}$ charge-conservation symmetries, and the conservation of total spin $\sum_{\boldsymbol{j}} S^z_{\boldsymbol{j}}$, the system exhibits hidden symmetries. Namely, when the holes move they only

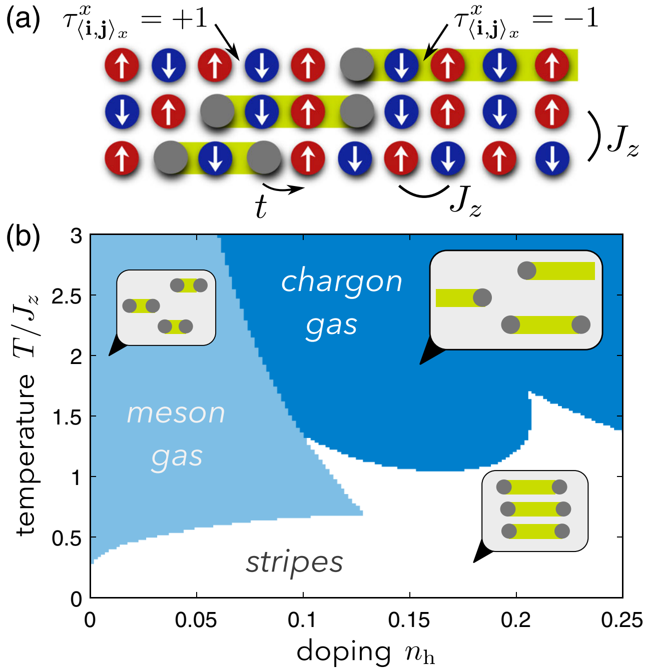

FIG. 1. The mix-D $t-J_z$ model with tunneling t along x and Ising couplings J_z in both directions can be mapped to coupled 1D $\mathbb{Z}_2$ LGTs. (a) With a classical Néel background the $\mathbb{Z}_2$ electric field lines $\tau^x_{\langle i,j\rangle_x} = -1$ denote regions where spins switch sublattice. (b) The phase diagram (here parton mean-field results for $t/J_z = 3$ are shown) contains stripes, a confined meson gas, and a deconfined chargon gas.

change the positions of the spins in the 2D lattice, while it is impossible to permute their configurations within any given chain. This is formalized by the notion of squeezed space, introduced to describe 1D doped spin chains [15,16]: To this end Fock states $\otimes_y |\sigma_{(1,y)}, \ldots, \sigma_{(L_x-1,y)}, \sigma_{(L_x,y)}\rangle$, with $\sigma_j = \uparrow, h, \downarrow$ denoting local spin and charge configurations, are relabeled by $\otimes_y |\tilde{\sigma}_{(1,y)}, \ldots, \tilde{\sigma}_{(\tilde{L}_x,y)}\rangle \otimes \hat{h}^\dagger_{(x_1,y)} \ldots \hat{h}^\dagger_{(x_{N^h_y},y)}|0\rangle$; Now $\tilde{\sigma}_j = \uparrow, \downarrow$ denotes spins only on sites $\tilde{x} = 1 \ldots \tilde{L}_x = L_x - N^h_y$ and $\hat{h}^\dagger_j$ creates a hard-core chargon with the same statistics as $\hat{c}_{j,\sigma}$ on the sites occupied by holes. The spin states in squeezed space are related to spins in the lattice by

$$\tilde{\sigma}(\tilde{x}, y) = \sigma\left(\tilde{x} + \sum_{j<\tilde{x}} n^h_{(j,y)}, y\right) \neq h, \tag{2}$$

where n^h_j denotes the chargon occupation numbers.

After this relabeling, the eigenfunctions of Eq. (1) become $|\Psi\rangle = |\tilde{\Psi}\rangle \otimes |\Psi_c\rangle$, where $|\tilde{\Psi}\rangle = |\{\tilde{\sigma}_{\tilde{j}}\}_{\tilde{j}}\rangle$ denotes a Fock configuration of spins in squeezed space and $|\Psi_c\rangle$ is a (generally correlated) chargon wave function [15]. Since we consider classical Ising interactions, every Fock configuration $|\tilde{\Psi}\rangle$ defines a separate hidden-symmetry sector of $\hat{\mathcal{H}}$. In the following we restrict ourselves to Néel states in squeezed space: $|\tilde{\Psi}\rangle = |N\rangle \equiv |\ldots\uparrow\downarrow\uparrow\ldots\rangle$, with long-range antiferromagnetic correlations along the x and y directions.

If projected to the subspace $|\tilde{\Psi}\rangle = |N\rangle$, the Hamiltonian for the chargons (with density $\hat{n}^h_j = \hat{h}^\dagger_j \hat{h}_j$) becomes

$$\hat{\mathcal{H}} = -t \sum_{\langle i,j\rangle_x} (\hat{h}^\dagger_i \hat{h}_j + \mathrm{H.c.}) + \hat{\mathcal{H}}_{\mathrm{int}}[\{\hat{n}^h_j\}], \tag{3}$$

where the sign of the tunneling term is irrelevant.

To express the nonlocal (but instantaneous) interaction energy $\hat{\mathcal{H}}_{\mathrm{int}}[\{\hat{n}^h_j\}]$ in a compact form, we introduce the following string operators,

$$\hat{\tau}^x_{\langle j,j+e_x\rangle_x} = \prod_{i:\, i_x \leq j_x} (-1)^{\hat{n}^h_i}. \tag{4}$$

By definition, each pair of holes is connected by a string of link variables $\tau^x_{\langle i,j\rangle} = -1$ [see Fig. 1(a)] and the following $\mathbb{Z}_2$ Gauss law is satisfied for all sites j:

$$\hat{G}_j|\Psi\rangle = |\Psi\rangle, \qquad \hat{G}_j = \prod_{i:\langle i,j\rangle_x} \hat{\tau}^x_{\langle i,j\rangle_x}. \tag{5}$$

Owing to this Gauss law, the two link variables including a site j occupied by a spin σ_j are equal, $\tau^x_{\langle j-e_x,j\rangle_x} = \tau^x_{\langle j,j+e_x\rangle_x} = (-1)^{\pi_j}$. Their value is given by the sublattice parity $\pi_j = 0, 1$ of this spin, i.e., the number of times mod 2 the spin has switched sublattice (starting from a Néel state with all holes located on the right edge).

The Ising interaction between neighboring spins $\langle i,j\rangle_y$ along y can be expressed in terms of the sublattice parities, $J_z \hat{S}^z_i \hat{S}^z_j = -J_z(-1)^{\pi_i+\pi_j}/4$, since we use $|\tilde{\Psi}\rangle = |N\rangle$. Along the chains each bond $\langle i,j\rangle_x$ gives $J_z \hat{S}^z_i \hat{S}^z_j = -J_z/4$ unless one of the sites is occupied by a chargon.

We proceed by promoting the link variables to a $\mathbb{Z}_2$ lattice gauge theory (LGT) subject to the $\mathbb{Z}_2$ Gauss law (5). This requires adding a term $\hat{\tau}^z_{\langle i,j\rangle_x}$ in the tunneling term in Eq. (3) which correctly flips the sign of $\tau^x_{\langle i,j\rangle_x}$, i.e., $\hat{\tau}^z_{\langle i,j\rangle_x}|\tau^x_{\langle i,j\rangle_x}\rangle = |-\tau^x_{\langle i,j\rangle_x}\rangle$. Note that the $\mathbb{Z}_2$ electric field $\hat{\tau}^x_{\langle i,j\rangle_x}$ has a concrete physical meaning as it can be measured from the local spin configuration.

Finally, we arrive at the exact representation of Eq. (1), in the sector $|\tilde{\Psi}\rangle = |N\rangle$, by a $\mathbb{Z}_2$ LGT,

$$\begin{aligned}\hat{\mathcal{H}} = &-A\frac{J_z}{4} - t\sum_{\langle i,j\rangle_x} (\hat{h}^\dagger_i \hat{\tau}^z_{\langle i,j\rangle_x} \hat{h}_j + \mathrm{H.c.}) + \frac{J_z}{2}\sum_j \hat{n}^h_j \\ &- \frac{J_z}{4}\sum_{\langle i,j\rangle_x} \hat{n}^h_i \hat{n}^h_j - \alpha\frac{J_z}{8}\sum_{\langle i,j\rangle_y} (1-\hat{n}^h_i)(1-\hat{n}^h_j) \\ &[\hat{\tau}^x_{\langle i-e_x,i\rangle_x}\hat{\tau}^x_{\langle j-e_x,j\rangle_x} + \hat{\tau}^x_{\langle i,i+e_x\rangle_x}\hat{\tau}^x_{\langle j,j+e_x\rangle_x}],\end{aligned} \tag{6}$$

where $A = L_x L_y$ is the total area. We introduced the dimensionless interchain coupling parameter α, which is $\alpha = 1$ for our model in Eq. (1).

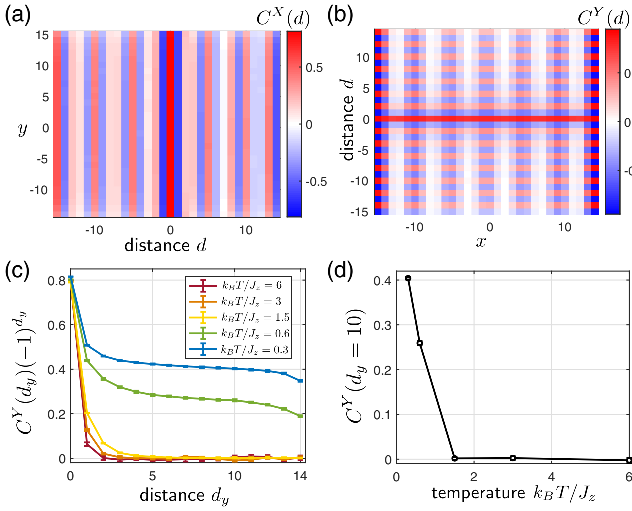

FIG. 2. Stripe formation: QMC simulations of Eq. (6) reveal the onset of stripe order at low temperatures. We show $C^X(d)$ in (a) [$C^Y(d)$ in (b)] relative to the central column (chain) at $d = 0$ for $k_BT = 0.6J_z$. (c) For different temperatures we show how long-range AFM spin correlations $(-1)^d C^Y(d)$ develop perpendicular to the chains; $C^Y(d)$ is measured relative to the central chain. The correlator at a large distance $d = 10$ is shown in (d). We consider a 30×30 system (open boundaries), 6 holes per chain, and $t/J_z = 3$.

Many-body phase diagram.—Figure 1(b) shows the phase diagram of the model in Eq. (6) as a function of temperature k_BT and doping n_h. The phase boundaries are estimated using a parton-based mean-field description; note that our calculations for the stripe and meson regimes are restricted to low enough dopings to assume pointlike constituents, which leads to unphysical cusps and reentrances associated with stripes. See Ref. [17] for details. Each phase is also found in our quantum Monte Carlo (QMC) simulations.

For the ground state ($T = 0$) we predict a vertical stripe phase, characterized by charge modulations with wavelength $\lambda = 1/n_h$. The $\mathbb{Z}_2$ electric field changes sign across each stripe, respecting the $\mathbb{Z}_2$ Gauss law.

As a result, incommensurate long-range spin correlations are found along x, see Fig. 2(a):

$$C^X(d) \equiv 4\langle \hat{S}^z_{\boldsymbol{j}} \hat{S}^z_{\boldsymbol{j}+d\boldsymbol{e}_x} \rangle \simeq \nu^X_S \cos[\pi(1+n_h)d], \quad d \to \infty. \tag{7}$$

The binding mechanism into stripes can be readily understood from Eq. (6): The interactions of the $\mathbb{Z}_2$ electric field lines favor alignment of the latter along y, which is achieved by creating strong charge correlations along the y direction. Such localization along y is cheap due to the absence of chargon tunneling in this direction. On the other hand, strong antibunching along x allows each chargon to delocalize as much as possible, in direct competition with the attraction of $\mathbb{Z}_2$ electric field lines.

As shown in Fig. 2(b), stripes are indeed characterized by long-range AFM order in the y direction (corresponding to aligned $\mathbb{Z}_2$ electric field lines):

$$C^Y(d) \equiv 4\langle \hat{S}^z_{\boldsymbol{j}} \hat{S}^z_{\boldsymbol{j}+d\boldsymbol{e}_y} \rangle \simeq \nu^Y_S (-1)^d, \qquad d \to \infty. \tag{8}$$

Numerically, we find that long-ranged correlations $C^Y(d)$ develop below a nonzero critical temperature $T_S > 0$. Our QMC simulations in Figs. 2(c) and 2(d) show that $k_BT_S \approx 1.0(5)J$ for the chosen value of $t/J_z = 3$ and 20% hole doping for linear system size $L = 15$.

Within each chain our system has a conserved number of holes, associated with separate $U(1)$ symmetries. In the long-wavelength limit, the corresponding effective field theory describes a $U(1)$ symmetric field without quantum fluctuations of the charge along y. Integrating out thermal fluctuations at temperatures $k_BT > 0$ yields an effective action of a $1+1$ dimensional quantum system. With the global $U(1)$ symmetry along y, we thus expect power-law correlations along x and y in the stripe phase: Below the critical temperature for stripe formation, $T_S > 0$, these replace the infinite-range correlations Eqs. (7), (8) expected in the true ground state.

We find that our finite-size simulations with open boundaries are consistent with very weak power-law correlations $C^Y(d)$ when $0 < T \lesssim T_S$. The detailed nature of the transition at T_S remains a subject of future investigation, but we expect it to be in the BKT class.

At higher temperatures and beyond a rather small critical doping value $n_h \geq n^c_h(T)$ we predict a chargon gas. It has no long-range AFM order in either direction, $C^X(d)$, $C^Y(d) \to 0$ as $d \to \infty$. The loss of antiferromagnetism is entirely due to chargon dynamics, however: in squeezed space the spin wave function is still the classical Néel state. Hence the chargon gas is characterized by its hidden AFM order, which manifests itself in the nonlocal string correlations defined by the $\mathbb{Z}_2$ Gauss law (5). Related string correlations have been observed in 1D Hubbard models [9,22] and are commonly used to characterize topological order in 1D systems [23,24].

In contrast to the stripe phase, the chargon gas is characterized by a *disordered* $\mathbb{Z}_2$ electric field:

$$e_{\langle \boldsymbol{i},\boldsymbol{j}\rangle_x} \equiv \langle \hat{\tau}^x_{\langle \boldsymbol{i},\boldsymbol{j}\rangle_x} \rangle = 0. \tag{9}$$

Chargons are hence deconfined and form a gapless phase [25], corresponding to free fermionic holes at the mean-field level.

Finally, at very low doping $n_h < n^c_h(T)$, but above the critical temperature $T > T_S(n_h)$ for stripe formation, we predict a meson gas. It is characterized by a uniform $\mathbb{Z}_2$ electric order parameter

$$e_{\langle \boldsymbol{i},\boldsymbol{j}\rangle_x} \equiv \langle \hat{\tau}^x_{\langle \boldsymbol{i},\boldsymbol{j}\rangle_x} \rangle = \nu_{\mathrm{cc}} \neq 0. \tag{10}$$

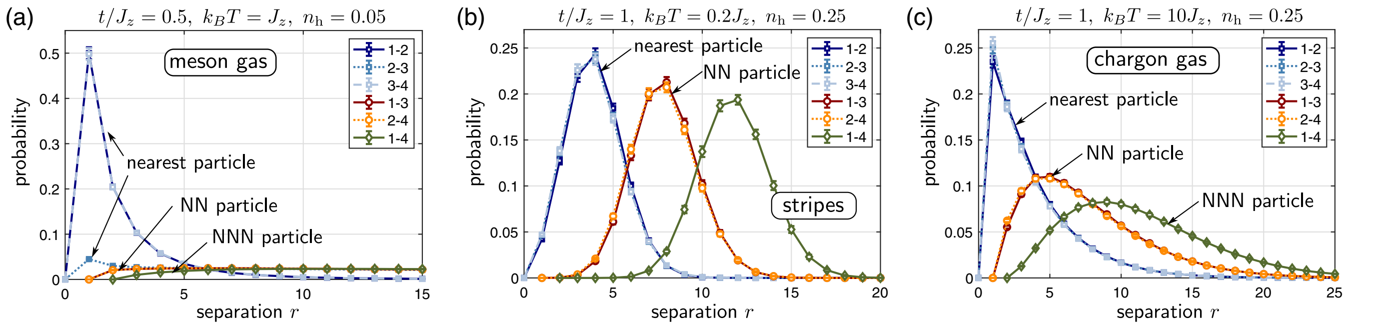

FIG. 3. Chargon distance histograms. We plot the distributions $p_{n,m}(r)$ of separations r between chargons number n and m in the chains, counting from the left. In the meson gas phase (a) $p_{1,2}(r) = p_{3,4}(r)$ is significantly broader than $p_{2,3}(r)$, a direct indication for pairing. In the stripe phase (b), $p_{1,2}(r) = p_{2,3}(r) = p_{3,4}(r) = \ldots$ are equal and all distributions are narrow, indicating localization of chargons into stripes. (c) In the chargon gas phase, $p_{1,2}(r) = p_{2,3}(r) = p_{3,4}(r) = \ldots$ and all distributions feature long tails. In all simulations we used an 80×10 system (other parameters as indicated).

This should be contrasted to the $T = 0$ stripe phase with incommensurate magnetism, where $e_{\langle i,j\rangle_x} \neq 0$ is modulated in space with a wavelength $\lambda = 2/n_h$, such that $\sum_{\langle i,j\rangle} e_{\langle i,j\rangle_x} = 0$; in the stripe phase at $0 < T < T_S$ the thermal average $e_{\langle i,j\rangle_x} = 0$ is expected to be strictly zero in the thermodynamic limit. As a direct consequence of $\nu_{cc} \neq 0$, the meson gas has commensurate long-range AFM order along both directions,

$$C^X(d), \qquad C^Y(d) \to (-1)^d \nu_{cc}^2, \qquad d \to \infty. \tag{11}$$

Physically, the meson gas can be understood as a paired phase of chargons. The $\mathbb{Z}_2$ electric string connecting two chargons is associated with a linear string tension $\propto \nu_{cc}$, which precludes one-chargon excitations in the thermodynamic limit; i.e., the meson gas corresponds to a confined phase which has, even in the zero-temperature limit, $\langle \hat{h}_j^\dagger (\prod_{j \le \langle i,k\rangle_x \le j+de_x} \hat{\tau}^z_{\langle i,k\rangle_x}) \hat{h}_{j+de_x} \rangle \simeq e^{-\eta d}$ for $d \to \infty$. Because of the restriction of chargon dynamics along one direction, the meson gas also corresponds to a Luttinger liquid with fractionalized excitations in the zero-temperature limit [25].

To identify the meson gas phase in our QMC numerics, we calculate histograms of chargon separations in Fig. 3. The hallmark of chargon-chargon meson formation is a narrow distribution $p_{2n-1,2n}(r)$ of separations r between chargon numbers $2n - 1$ and $2n$, with $n = 1, 2, \ldots$ and counting from the left edge, and a broader and different distribution $p_{2n,2n+1}(r)$ between chargons $2n$ and $2n + 1$. This feature is clearly visible in Fig. 3(a) in the expected low-doping regime, where we also find a nonvanishing $\mathbb{Z}_2$ electric order parameter, $\langle \hat{\tau}^x_{\langle i,j\rangle_x} \rangle = 0.8842(8)$. In the other two phases, the histograms show significantly different features, see Figs. 3(b), 3(c).

In the phase diagram, the meson gas is associated with an unusual reentrant behavior as one increases temperature along a line of constant, but small, doping: at $T = 0$ the system has incommensurate long-range AFM correlations, which we predict to be destroyed by thermal fluctuations of the stripes when $0 < T < T_S$. When the meson gas phase is entered for $T > T_S$, true long-range AFM correlations are restored. This counterintuitive behavior is possible since AFM correlations are merely hidden in the intermediate fluctuating stripe regime.

Finally, we want to make a connection with Ref. [14], where a single mobile dopant but with $SU(2)$ invariant Heisenberg interactions has been studied. It was found that the hole forms a magnetic polaron [5,26–28] that can be understood as a mesonlike bound state of a spinon and a chargon [29] connected by a geometric string of displaced spins [14]. Our meson phase is an analog of this finding but at finite hole concentration and for Ising-type interactions.

Methods.—Our calculations are based on a number of different but standard techniques such as bosonization, mean-field parton theory, and QMC simulations.

In order to work with a 1D field theory amenable to bosonization, our crucial approximation is the decoupling ansatz

$$\hat{\tau}^x_{\langle i,i+e_x\rangle_x} \hat{\tau}^x_{\langle j,j+e_x\rangle_x} \approx V_{\mathrm{MF}}(i_x)[\hat{\tau}^x_{\langle i,i+e_x\rangle_x} + \hat{\tau}^x_{\langle j,j+e_x\rangle_x}], \tag{12}$$

for $\langle i,j\rangle_y$ NN along y, i.e., $i_x = j_x$. The different phases correspond to different solutions for $V_{\mathrm{MF}}(i_x)$. These approximations are justified because we find the same phases in the quantum Monte Carlo simulations. We find the critical Luttinger parameter below which the ground state forms stripes to be large, $K_c = 8$. We refer to the Supplemental Material [17] for details.

Discussion and outlook.—In summary, we showed that the mix-D $t - J_z$ model can be directly mapped onto a $\mathbb{Z}_2$ LGT. The many-body phase diagram of our model features in the ground state a stripe phase where the holes form vertical walls. Above a critical temperature T_S, but within the Néel $\mathbb{Z}_2$ gauge sector (which has the lowest energy at zero doping), we find two gaseous phases: a confined meson gas, with long-range AFM order, and a deconfined chargon gas with hidden AFM correlations.

Experimentally, the model Eq. (1) can be realized in the large U/t limit of a bosonic Hubbard model with a strong tilt $\Delta \gg t$ along the y direction: The strong tilt suppresses resonant tunneling of dopants along y, whereas the superexchange mechanism remains intact in both directions 14,30]]; to obtain AFM Ising interactions, one can use spin-dependent scattering lengths [30,31]. Rydberg atoms, which have already demonstrated Ising spin systems [32–37], are an alternative option: By using multiple hyperfine levels to encode both spin and charge degrees of freedom, our mix-D $t-J_z$ model should also be realizable; see also Ref. [38] for a discussion of generic $t-XYZ$ models in polar molecules, and Refs. [39–42] for direct implementations of $\mathbb{Z}_2$ LGTs. For all systems, we propose to start from a classical Néel state without holes, which can be doped with mobile charges, e.g., by adiabatic deformations of the trapping potentials. This should guarantee that thermal fluctuations outside the gauge sector of our $\mathbb{Z}_2$ LGT are negligible.

In spite of the overwhelming simplifications of our model, the presence of a stripe phase and a confinement-to-deconfinement transition at elevated temperatures draws one's attention to the cuprates. A goal for future investigations is to study related models which are more closely related to the 2D $t-J$ model: as a first step, other gauge sectors with domain walls in squeezed space—corresponding to spinons—can be considered. By replacing Ising interactions with $SU(2)$ invariant Heisenberg couplings, a much richer model is expected and it remains to be seen if any connections to $\mathbb{Z}_2$ LGTs can be drawn. Finally, the goal is to include charge dynamics along the second direction: this may provide an adiabatic route to the stripe phase observed in cuprates.

Numerical data for this Letter are available [43].

We thank J. Amato-Grill, L. Barbiero, I. Bloch, A. Bohrdt, U. Borla, M. Buser, P. Cubela, E. Demler, I. Dimitrova, S. Eggert, N. Goldman, M. Greiner, C. Gross, N. Jepsen, M. Kebric, J. Koepsell, S. Moroz, M. Punk, G. Salomon, U. Schollwöck, T. Shi, R. Verresen, and Z. Zhu for fruitful discussions. We acknowledge funding by the Deutsche Forschungsgemeinschaft (DFG, German Research Foundation) under Germany's Excellence Strategy—EXC-2111–390814868 and via Research Unit FOR 2414 under Project No. 277974659. L. P. is supported by FP7/ERC Consolidator Grant No. 771891 (QSIMCORR).

[1] A. Mazurenko, C. S. Chiu, G. Ji, M. F. Parsons, M. Kanasz-Nagy, R. Schmidt, F. Grusdt, E. Demler, D. Greif, and M. Greiner, A cold-atom Fermi-Hubbard antiferromagnet, Nature (London) **545**, 462 (2017).

[2] P. T. Brown, D. Mitra, E. Guardado-Sanchez, P. Schauss, S. S. Kondov, E. Khatami, T. Paiva, N. Trivedi, D. A. Huse, and W. S. Bakr, Spin-imbalance in a 2D Fermi-Hubbard system, Science **357**, 1385 (2017).

[3] P. T. Brown, D. Mitra, E. Guardado-Sanchez, R. Nourafkan, A. Reymbaut, C.-D. Hebert, S. Bergeron, A.-M. S. Tremblay, J. Kokalj, D. A. Huse, P. Schauß, and W. S. Bakr, Bad metallic transport in a cold atom Fermi-Hubbard system, Science **363**, 379 (2019).

[4] M. A. Nichols, L. W. Cheuk, M. Okan, T. R. Hartke, E. Mendez, T. Senthil, E. Khatami, H. Zhang, and M. W. Zwierlein, Spin transport in a Mott insulator of ultracold fermions, Science **363**, 383 (2019).

[5] J. Koepsell, J. Vijayan, P. Sompet, F. Grusdt, T. A. Hilker, E. Demler, G. Salomon, I. Bloch, and C. Gross, Imaging magnetic polarons in the doped Fermi-Hubbard model, Nature (London) **572**, 358 (2019).

[6] G. Ji, M. Xu, L. H. Kendrick, C. S. Chiu, J. C. Brüggenjürgen, D. Greif, A. Bohrdt, F. Grusdt, E. Demler, M. Lebrat, and M. Greiner, Dynamical interplay between a single hole and a Hubbard antiferromagnet, arXiv:2006.06672v1.

[7] C. S. Chiu, G. Ji, A. Bohrdt, M. Xu, M. Knap, E. Demler, F. Grusdt, M. Greiner, and D. Greif, String patterns in the doped Hubbard model, Science **365**, 251 (2019).

[8] A. Bohrdt, C. S. Chiu, G. Ji, M. Xu, D. Greif, M. Greiner, E. Demler, F. Grusdt, and M. Knap, Classifying snapshots of the doped Hubbard model with machine learning, Nat. Phys. **15**, 921 (2019).

[9] T. A. Hilker, G. Salomon, F. Grusdt, A. Omran, M. Boll, E. Demler, I. Bloch, and C. Gross, Revealing hidden antiferromagnetic correlations in doped Hubbard chains via string correlators, Science **357**, 484 (2017).

[10] J. Vijayan, P. Sompet, G. Salomon, J. Koepsell, S. Hirthe, A. Bohrdt, F. Grusdt, I. Bloch, and C. Gross, Time-resolved observation of spin-charge deconfinement in fermionic Hubbard chains, Science **367**, 186 (2020).

[11] G. Salomon, J. Koepsell, J. Vijayan, T. A. Hilker, J. Nespolo, L. Pollet, I. Bloch, and C. Gross, Direct observation of incommensurate magnetism in Hubbard chains, Nature (London) **565**, 56 (2019).

[12] J. Zaanen, O. Y. Osman, H. V. Kruis, Z. Nussinov, and J. Tworzydlo, The geometric order of stripes and Luttinger liquids, Philos. Mag. B Phys. Condens. Matter **81**, 1485 (2001).

[13] M. Qin, C.-M. Chung, H. Shi, E. Vitali, C. Hubig, U. Schollwöck, S. R. White, and S. Zhang, Absence of Superconductivity in the Pure Two-Dimensional Hubbard Model, Phys. Rev. X **10**, 031016 (2020).

[14] F. Grusdt, Z. Zhu, T. Shi, and E. Demler, Meson formation in mixed-dimensional t-j models, SciPost Phys. **5**, 057 (2018).

[15] M. Ogata and H. Shiba, Bethe-ansatz wave function, momentum distribution, and spin correlation in the one-dimensional strongly correlated Hubbard model, Phys. Rev. B **41**, 2326 (1990).

[16] H. V. Kruis, I. P. McCulloch, Z. Nussinov, and J. Zaanen, Geometry and the hidden order of Luttinger liquids: The universality of squeezed space, Phys. Rev. B **70**, 075109 (2004).

[17] See Supplemental Material at http://link.aps.org/supplemental/10.1103/PhysRevLett.125.256401 for a description of the used methods, which includes Refs. [18–21].

[18] C. Prosko, S.-P. Lee, and J. Maciejko, Simple $\mathbb{Z}_2$ lattice gauge theories at finite fermion density, Phys. Rev. B **96**, 205104 (2017).

[19] T. Giamarchi, *Quantum Physics in One Dimension* (Oxford University Press, Oxford, 2003).

[20] N. V. Prokof'ev, B. V. Svistunov, and I. S. Tupitsyn, Exact, complete, and universal continuous-time worldline Monte Carlo approach to the statistics of discrete quantum systems, Sov. Phys. JETP **87**, 310 (1998).

[21] L. Pollet, K. Van Houcke, and S. M. A. Rombouts, Engineering local optimality in quantum Monte Carlo algorithms, J. Comput. Phys. **225**, 2249 (2007).

[22] M. Endres, M. Cheneau, T. Fukuhara, C. Weitenberg, P. Schauss, C. Gross, L. Mazza, M. C. Banuls, L. Pollet, I. Bloch, and S. Kuhr, Observation of correlated particle-hole pairs and string order in low-dimensional Mott insulators, Science **334**, 200 (2011).

[23] M. den Nijs and K. Rommelse, Preroughening transitions in crystal surfaces and valence-bond phases in quantum spin chains, Phys. Rev. B **40**, 4709 (1989).

[24] S. Fazzini, L. Barbiero, and A. Montorsi, Interaction-Induced Fractionalization and Topological Superconductivity in the Polar Molecules Anisotropic $t-j$ Model, Phys. Rev. Lett. **122**, 106402 (2019).

[25] U. Borla, R. Verresen, F. Grusdt, and S. Moroz, Confined Phases of One-Dimensional Spinless Fermions Coupled to z_2 Gauge Theory, Phys. Rev. Lett. **124**, 120503 (2020).

[26] C. L. Kane, P. A. Lee, and N. Read, Motion of a single hole in a quantum antiferromagnet, Phys. Rev. B **39**, 6880 (1989).

[27] S. Sachdev, Hole motion in a quantum néel state, Phys. Rev. B **39**, 12232 (1989).

[28] G. Martinez and P. Horsch, Spin polarons in the $t-j$ model, Phys. Rev. B **44**, 317 (1991).

[29] P. Beran, D. Poilblanc, and R. B. Laughlin, Evidence for composite nature of quasiparticles in the 2D $t-j$ model, Nucl. Phys. **B473**, 707 (1996).

[30] I. Dimitrova, N. Jepsen, A. Buyskikh, A. Venegas-Gomez, J. Amato-Grill, A. Daley, and W. Ketterle, Enhanced Superexchange in a Tilted Mott Insulator, Phys. Rev. Lett. **124**, 043204 (2020).

[31] L. M. Duan, E. Demler, and M. D. Lukin, Controlling Spin Exchange Interactions of Ultracold Atoms in Optical Lattices, Phys. Rev. Lett. **91**, 090402 (2003).

[32] P. Schauß, M. Cheneau, M. Endres, T. Fukuhara, S. Hild, A. Omran, T. Pohl, C. Gross, S. Kuhr, and I. Bloch, Observation of mesoscopic crystalline structures in a two-dimensional Rydberg gas, Nature (London) **491**, 87 (2012).

[33] P. Schauß, J. Zeiher, T. Fukuharaand, S. Hild, M. Cheneau, T. Macri, T. Pohl, I. Bloch, and C. Gross, Crystallization in ising quantum magnets, Science **347**, 1455 (2015).

[34] H. Labuhn, D. Barredo, S. Ravets, S. de Leseleuc, T. Macri, T. Lahaye, and A. Browaeys, Tunable two-dimensional arrays of single Rydberg atoms for realizing quantum Ising models, Nature (London) **534**, 667 (2016).

[35] H. Bernien, S. Schwartz, A. Keesling, H. Levine, A. Omran, H. Pichler, S. Choi, A. S. Zibrov, M. Endres, M. Greiner, V. Vuletić, and M. D. Lukin, Probing many-body dynamics on a 51-atom quantum simulator, Nature (London) **551**, 579 (2017).

[36] E. Guardado-Sanchez, P. T. Brown, D. Mitra, T. Devakul, D. A. Huse, P. Schauss, and W. S. Bakr, Probing Quench Dynamics Across a Quantum Phase Transition into a 2D Ising Antiferromagnet, Phys. Rev. X **8**, 021069 (2018).

[37] V. Lienhard, S. de Léséleuc, D. Barredo, T. Lahaye, A. Browaeys, M. Schuler, L.-P. Henry, and A. M. Läuchli, Observing the Space- and Time-Dependent Growth of Correlations in Dynamically Tuned Synthetic Ising Antiferromagnets, Phys. Rev. X **8**, 021070 (2018).

[38] A. V. Gorshkov, S. R. Manmana, G. Chen, J. Ye, E. Demler, M. D. Lukin, and A. M. Rey, Tunable Superfluidity and Quantum Magnetism with Ultracold Polar Molecules, Phys. Rev. Lett. **107**, 115301 (2011).

[39] E. Zohar, A. Farace, B. Reznik, and J. Ignacio Cirac, Digital Quantum Simulation of $\mathtt{F}_2$ Lattice Gauge Theories with Dynamical Fermionic Matter, Phys. Rev. Lett. **118**, 070501 (2017).

[40] C. Schweizer, F. Grusdt, M. Berngruber, L. Barbiero, E. Demler, N. Goldman, I. Bloch, and M. Aidelsburger, Floquet approach to $\mathbb{Z}_2$ lattice gauge theories with ultracold atoms in optical lattices, Nat. Phys. **15**, 1168 (2019).

[41] L. Barbiero, C. Schweizer, M. Aidelsburger, E. Demler, N. Goldman, and F. Grusdt, Coupling ultracold matter to dynamical gauge fields in optical lattices: From flux-attachment to $\mathbb{Z}_2$ lattice gauge theories, Sci. Adv. **5**, eaav7444 (2019).

[42] J. C. Halimeh and P. Hauke, Reliability of Lattice Gauge Theories, Phys. Rev. Lett. **125**, 030503 (2020).

[43] https://github.com/LodePollet/QSIMCORR.